# 4

# Dilute Nitride GaAsN and InGaAsN Layers Grown by Low-Temperature Liquid-Phase Epitaxy

Malina Milanova[1] and Petko Vitanov[2]
[1]*Central Laboratory of Applied Physics, BAS*
[2]*Central Laboratory of New Energy & New Energy Sources, BAS*
*Bulgaria*

## 1. Introduction

A critical goal for photovoltaic energy conversion is the development of high-efficiency, low cost photovoltaic structures which can reach the thermodynamic limit of solar energy conversion. New concepts aim to make better use of the solar spectrum than conventional single-gap cells currently do. In multijunction solar cells based on III-V heterostructures, better spectrum utilization is obtained by stacking several solar cells. These cells have achieved the highest efficiency among all other solar cells and have the theoretical potential to achieve efficiencies equivalent to or exceeding all other approaches. Record conversion efficiencies of 40.7 % (King, 2008) and 41,1 (Guter at al., 2009) under concentrated light for triple- junction allows hoping for practical realization of gianed values of efficiency in more multiplejunction structures. The expectations will be met , if suitable novel materials for intermediate cascades are found, and these materials are grown of an appropriate quality. Models indicate that higher efficiency would be obtained for 4-junction cells where 1.0 eV band gap cell is added in series to proven InGaP/GaAs/Ge triple-junction structures. Dilute nitride alloys such as GaInAsN, GaAsSbN provide a powerful tool for engineering the band gap and lattice constant of III-V alloys, due to their unique properties. They are promising novel materials for 4- and 5-junction solar cells performance. They exhibit strong bowing parameters and hold great potential to extend the wavelength further to the infrared part of the spectrum.

The incorporation of small quantity of nitrogen into GaAs causes a dramatic reduction of the band gap (Weyeres et al., 1992), but it also deteriorates the crystalline and optoelectronic properties of the dilute nitride materials, including reduction of the photoluminescence intensity and lifetime, reduction of electron mobility and increase in the background carrier concentration. Technologically, the incorporation probability of nitrogen in GaAs is very small and strongly depends on the growth conditions. GaAsN- based alloys and heterostructures are primarily grown by metaloorganic vapor-phase epitaxy (MOVPE) (Kurtz et all, 2000; Johnston et all, 2005)) and molecular-beam epitaxy (MBE) (Kurtz et al. 2002; Krispin et al, 2002; Khan et al, 2007), but the material quality has been inferior to that of GaAs. A peak internal quantum efficiency of 70 % is obtained for the solar cells grown by MOCVD (Kurtz et al. 1999). Internal quantum values near to unit are reported for p-i-n

GaInAsN cell grown by MBE (Ptak et al 2005), but photovoltages in this material are still low. Recently chemical-beam epitaxy (Nishimura et al., 2007; Yamaguchi et al, 2008; Oshita et al, 2011) has been developed in order to improve the quality of the grown layer, but today it remains a challenge to grow dilute nitride materials with photovoltaic (PV) quality.
In this chapter we present some results on thick GaAsN and InGaAsN layers, grown by low-temperature Liquid-Phase Epitaxy (LPE). In the literature there are only a few works on dilute nitride GaAsN grown by LPE (Dhar et al., 2005; Milanova et al., 2009) and some data for InGaAsN (Vitanov et al., 2010).

## 2. Heteroepitaxy nucleation and growth modes

The mechanism of nucleation and initial growth stage of heteroepitaxy dependence on bonding between the layer and substrate across the interface. Since the heteroepitaxy requires the nucleation of a new alloy on a foreign substrate the surface chemistry and physics play important roles in determining the properties of heteroepitaxial growth. In the classical theory, the mechanism of heterogeneous nucleation is determined by the surface and interfacial free energies for the substrate and epitaxial crystal.
Three classical modes of initial growth introduced at first by Ernst Bauer in 1958 can be distinguished: Layer by layer or Frank–Van der Merwe FM two-dimension mode (Frank–Van der Merwe, 1949), Volmer–Weber VW 3D island mode (Volmer–Weber, 1926), and Stranski–Krastanov SK or layer-plus-island mode (Stranski–Krastanov, 1938) as the intermediate case. The layer by layer growth mode arises when dominates the interfacial energy between substrate and epilayer material. In the opposite case, for the weak interfacial energy when the deposit atoms are more strongly bound to each other than they are to the substrate, the island (3D), or VW mode results. In the SK case, 3D island are formed on several monolayers, grown in a layer-by-layer on a crystal substrate.
Schematically these growth modes are shown in the Figure 2.1.

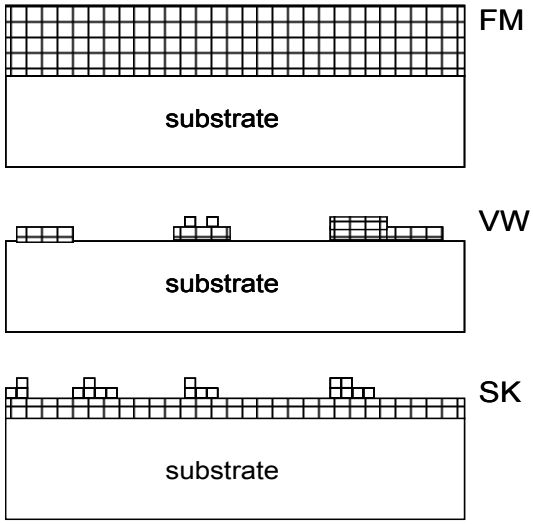


Fig. 2.1. Schematic presentation of FM, VW and SK growth modes

The growth modes in heteroepitaxy are defined based on thermodynamic models.
The sum of the film surface energy and the interface energy must be less than the surface energy of the substrate in order for wetting to occur and then layer by layer growth is expected. The VW growth mode is to be expected for a no wetting epitaxial layer. If $\gamma$ and $\gamma_0$ are the surface free energies of the layer and substrate, respectively, and $\gamma_i$ is the interfacial free energy the change in the free energy $\Delta\gamma$ associated with covering the substrate with epitaxial layer is:

$$\Delta\gamma = \gamma + \gamma_i - \gamma_0 \tag{2.1}$$

If minimum energy determinates the mode for nucleation and growth, the dominated mechanism will be two-dimensional for $\Delta\gamma < 0$ and three-dimensional for $\Delta\gamma > 0$. However, even in the case of a wetting epitaxial layer ($\Delta\gamma < 0$ ), the existence of mismatch strain can cause islanding after the growth of a few monolayers. This is because the strain energy , increases linearly with the number of strained layers. At some thickness, $\gamma+\gamma i$ exceeds $\gamma_0$ and the growth mode transforms from FM to SK resulting in 3D islands on the 2D wetting layer. Whereas it is clear that the VW growth mode is expected for a nonwetting epitaxial layer, the behavior of a wetting deposit is more complex and requires further consideration. Often the interfacial contribution in the limit of zero lattice mismatch and weak chemical interactions between the film and substrate at the interface can be neglected in comparison to the surface free energy ($\gamma i \approx 0$). In this case the growth mode is determined entirely by the surface free energies of the film and substrate material.
Instead of these three main growth modes additional growth modes and epitaxial growth mechanisms could be distinguished (Scheel, 2003): columnar growth, step flow mode, step bunching, and screw-island growth.
The structural quality of the layer and surface morphology strongly depend on the growth method and the main growth parameters: supersaturation, misorientation of the substrate and the difference of lattice constants between substrate and the epitaxial layer.
In the case of flat substrate, the supersaturation increases until surface nucleation of a new monolayer occurs and its growth cover the substrate, followed by the nucleation of the next monolayer. For compound of limited thermodynamic stability or with volatile constituents like GaAs, GaN, SiC the appearance of the growth mode is largely predetermined by the choice of the growth method due to the inherent high supersaturation in epitaxy from the vapor phase and adjustable low supersaturation in LPE.
The FM growth mode in LPE can only be obtained at quasi-zero misfit as it is established from thermodynamic theory (Van der Merwe, 1979) and demonstrated by atomistic simulations using the Lennard–Jones potential (Grabow and Gilmer, 1988) and also at low supersaturation. At high supersaturation a high thermodynamic driving force leads to a high density of steps moving with large step velocities over the surface and causes step bunching.
The VW mode is typical of VPE. Due to the high supersaturation a large number of surface nuclei arise, which then spread and form three-dimensional islands, that finally coalesce to a compact layer. Continued growth of a layer initiated by the VW mode often shows columnar growth which is a common feature in epitaxy of GaN and diamond. (Hiramatsu *et al*., 1991). The SK mode has been demonstrated by MBE growth of InAs onto GaAs substrate (Nabetani *et al*., 1994).

Observations, analyses and measurements of LPE GaAs on the formation of nuclei and surface terraces show that nuclei grow into well-defined prismatic hillocks bounded by only {100} and {111} planes and they are unique to each substrate orientation, and hillocks tend to coalesce into chains and then into parallel surface terraces (Mattes & Route, 1974). The hillock boundaries may cause local strain fields and variation of the incorporation rates of impurities and dopants, or the local strain may getter or rejects impurities during annealing processes. This inhomogeneity may be suppressed by providing one single step source or by using substrates of well-defined small misorientation. The FM growth mode and such homogeneous layers can only be achieved by LPE or by VPE at very high growth temperatures.

Only at low supersaturation, nearly zero misfit and small misorientation of the substrate the layer by-layer growth mode can be realized and used to produce low dislocation layers for ultimate device performance. Two-dimensional growth is desirable because of the need for multilayered structures with flat interfaces and smooth surfaces. A notable exception is the fabrication of quantum dot devices, which requires three-dimensional or SK growth of the dots. Even here it is desirable for the other layers of the device to grow in a two-dimensional mode. In all cases of heteroepitaxy, it is important to be able to control the nucleation and growth mode.

## 3. Pseudomorphic and metamorphic growth

One of the main requirements for high quality heterostructure growth is the lattice constant of the growth material to be nearly the same as those of the substrate. In semiconductor alloys the lattice constant and band gap can be modified in a wide range. The lattice parameter difference may vary from nearly 0 to several per cent as in the cases of GaAs-AlAs and InAs-GaAs system, respectively. The growth of dilute nitride alloys is difficult because of the wide immiscibility range, a large difference in the lattice constant value and very small atom radius of N atoms. The growth of thick epitaxial layers creates many problems which absent in the quantum-well structures.

At the initial stage of the growth when the epitaxial layer is of different lattice constant than the substrate in-plane lattice parameter of the growth material will coherently strain in order to match the atomic spacing of the substrate. The elastic energy of deformation due to the misfit in lattice constant destroys the epilayer lattice. The substrate is sufficiently thick and it remains unstrained by the growth of the epitaxial layer. If the film is thin enough to remain coherent to the substrate, then in the plane parallel to the growth surface, the thin film will adopt the in-plane lattice constant of the substrate, i.e. $a_{II} = a_o$, where $a_{II}$ is the in-plane lattice constant of the layer and $a_o$ is the lattice constant of the substrate. This is the case of pseudomorphic growth, and the epitaxial layer is pseudomorphic. If the lattice constant of the layer is larger than that of the substrate as in the case of InGaAs on GaAs, under the pseudomorphic condition growth the lattice of the layer will be elastically compressed in the two in-plane directions. The lattice constant of the layer in the growth direction perpendicular to the interface (the so-called out-of plane direction) will be strained according the Poison effect and will be larger than the unstrained value and the layer lattice will tense in the growth direction. Schematically this situation is illustrated in Figure 3.1.

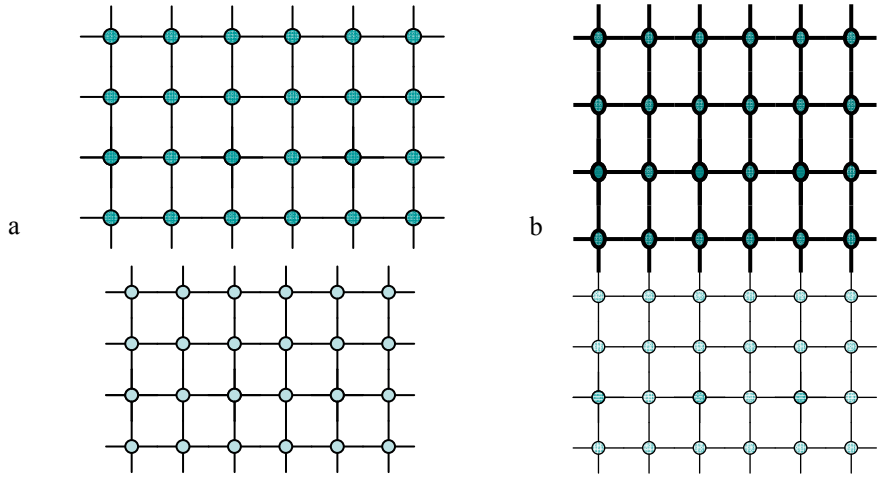


Fig. 3.1. Schematic presentation of atom arrangement for two materials with different cubic lattice constant: a) before growth; b) for pseudomorphic growth

In the case of the smaller lattice constant of the growth layer (GaAsN on GaAs for example), $a < a_o$ the layer will be elastically tensed in two in-plane directions and compressed in the growth directions (the out-of-plane lattice constant will be smaller than substrate lattice constant). Under pseudomorphic growth conditions the cubic lattice doesn't remain cubic: $a_{II} = a_o \neq a_\perp$. The out -of-plane lattice constant could be determined from the equation:

$$a_\perp = a[1 - D(a_{II}/a - 1)] \tag{3.1}$$

Where:
$a_\perp$ - out-of-plane lattice constant of the layer
$a_{II}$ - in-plane lattice constant of the layer
$a$ - lattice constant of the unstrained cubic epitaxial layer
$D = 2C_{12}/C_{11}$, where $C_{11}$ and $C_{12}$ are elastic constants of the grown layer
Beyond a given critical thickness $\eta_c$ when a critical misfit strain $\varepsilon$ is exceeded, a transition from the elastically distorted to the plastically relaxed configuration occurs. In this case both mismatch component differ from zero: $a_{II} \neq a_o \neq a_\perp$. The lattice constant misfit is:

$$f = (a - a_o)/a_o$$

$$f_\perp = (a_\perp - a_o)/a_o = (1+D-DR)f \tag{3.2}$$

$$f_{II} = (a_{II} - a_o)/a_o = Rf$$

$R$ is a relaxation rate. For pseudomorphic growth $R$=0, and for full strain relaxation $R$ =1
If the epilayer is thicker than the critical thickness, there will be sufficient strain energy in the layer to create dislocations to relieve the excess strain. The layer has now returned to its unstrained or equilibrium lattice parameters in both the in-plane and out-of-plane directions and the film to be 100% relaxed. Figure 3.2 shows schematically how a misfit dislocation can relieve strain in the heteroepitaxial structure.

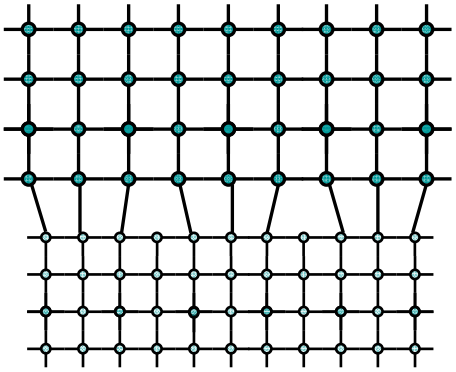

Fig. 3.2. Schematic presentation of the atom arrangement for metamorphic growth

In actual films, there is usually some amount of partial relaxation, although it can be very small in nearly coherent layers and nearly 100% in totally relaxed layers. For the partially relaxed layer, the in-plane lattice constant has not relaxed to its unstrained value. So some mismatch is accommodated by elastic strain, but a portion of the mismatch is accommodated by misfit dislocations (plastic strain).

There are two widely used models for calculations the critical thickness values: the Matthews-Blakeslee mechanical equilibrium model (Matthews.& Blakeslee, 1974) and the People-Bean energy equilibrium model (People & Bean, 1985). The People-Bean energy equilibrium model requires the total energy being at its minimum under critical thickness. According this model the elastic energy is equal to the dislocation energy at the critical thickness if the total elastic energy of the system with fully coherent interface is larger than the sum of the total system energy for the reduced misfit, due to the generation of dislocations, and the associated dislocation energy, and then begins the formation of interfacial dislocations.

Generally, the Matthews-Blakeslee model based on stemming from force balance, is the most often used to describe strain relaxation in thin films system. The equilibrium model of Matthews-Blakeslee assumes the presence of threading dislocations from the substrate. It gives mathematical relation for critical thickness by examining the forces originating from both the misfit strain $F_\varepsilon$ and the tension of dislocation line $F_L$. The critical thickness $h_c$ is defined as the thickness limit when the misfit strain force $F_\varepsilon$ is equal to the dislocation tension force $F_L$( at $h_c$ $F_\varepsilon = F_L$). For layers ticker than the critical thickness, the threading segment begins to glide and creates misfit dislocations at the interface to relieve the mismatch strain. The dislocations can easily move if dislocation lines and the Burgers vectors belong to the easy glide planes as {111} planes in face-centred cubic crystals.

In III-V semiconductors, the relaxation is known to occur by the formation of misfit dislocations and /or stacking faults. The usual misfit dislocations that are considered are located along the intersection of the glide plane and the interface plane. In zinc-blende crystal structures, on (100) oriented substrates the glide planes intersect the interface (110) which provides the corresponding line directions of misfit dislocations in such structures. The component of 60˚ dislocations perpendicular to the line directions contributes to strain relaxation. The 60˚ Burgers vector is b= ½ $a_1$ $\langle 110 \rangle$ and has a length along the interface perpendicular to the line $a / \sqrt{2}$ .

Calculated values for critical thickness from People-Bean energy equilibrium and Matthews-Blakeslee force balance models are:

$$h_c = \frac{b(1-\nu)}{32\pi f^2(1+\nu)}\ln(h_c / b) \tag{3.3}$$

$$h_c = \frac{b}{4\pi f(1+\nu)}[\ln(h_c / b)+1] \tag{3.4}$$

Where:
$\nu = C_{12}/(C_{12}+C_{11})$ is Poison's ratio,
$f$ is a lattice mismatch, $b = a/\sqrt{2}$ is a magnitude of Burgers vector
The calculated values of People-Bean models are larger than that of the Matthews-Blakeslee model. The measurements of dislocation densities in many cases showed no evidence of misfit dislocations for layer considerable ticker than Matthews-Blakeslee limit and nearly close to the energy-equilibrium thickness limit. Layers with thicknesses above the People-Bean limit can be considered to be completely relaxed, whereas layers below Matthews-Blakeslee limit values fully strained. Layers with thicknesses between these limits are metastable. They could be free of dislocations after growth, but are susceptible to relaxation during later high-temperature processing.
For the semiconductor devices based on the thick metamorphic structure the influence of the misfit dislocations which are located at the interface on active region could be reduced by growing the additional barrier layers before active region growth. Threading dislocations, which propagate up through the structure, are the most trouble for electronic devices since they can create defect states such as nonradiative centres and destroy the device properties.
There are a variety of techniques used to reduce the density of threading dislocations in a material. For planar structure a thick buffer layer with lattice parameter equal to that of the active layers is usually used for reduction of threading dislocations. However, these structures always have high threading dislocation densities. In most thick nearly relaxed heteroepitaxial layers, it is found that the threading dislocation density greatly exceeds that of the substrate. Some authors (Sheldon et al.1988, Ayers et al. 1992) are noted for a number of heteroepitaxial material systems that this dislocation density decreases approximately with the inverse of the thickness. The dislocation density could be reduced by postgrowth annealing.
A linearly graded buffers and graded superlattice also are effectively used for restricting dislocations to the plane parallel to the growth surface, and thus support the formation of misfit dislocation and suppress threading dislocation penetration in the active region.

### 3.1 X-ray diffraction characterization

The X-ray diffraction (XRD) method is an accurate nondestructive method for characterization of epitaxial structures. X-ray scans may be used for determination the lattice parameter, composition, mismatch and thicknesses of semiconductor alloys.
In XRD experiment a set of crystal lattice planes (hkl) is selected by the incident conditions and the lattice spacing $d_{hkl}$ is determined through the well-known Brag's law:

$$2d\sin\theta_B = n\lambda \tag{3.1.1}$$

where n is the order of reflection and $\theta_B$ is the Brag angle
The crystal surface is the entrance and exit reference plane for the X-ray beams in Bragg scattering geometry and the incident and diffracted beams make the same angle with the lattice planes. Two types of rocking curve scan are used: symmetric when the Bragg diffraction is from planes parallel to crystal surface and asymmetric when the diffraction lattice planes are at angle φ to the crystal surface (Fig. 3.3).

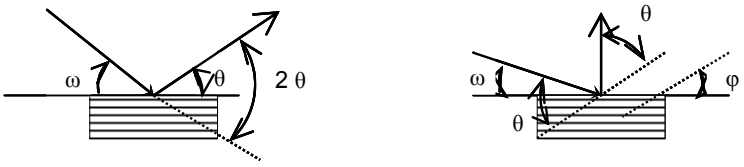


Fig. 3.3. Symmetric and asymmetric reflections from crystal surface

Let $\omega$ be the incidence angle with respect to the sample surface of a monochromatic X-ray beam. By rocking a crystal through a selected angular range, centered on the Bragg angle of a given set of lattice planes a diffraction intensity profile I($\omega$**)** is collected. For single layer heterostructure, the intensity profile will show two main peaks corresponding to the diffraction from the layer and substrate. The angular separation $\Delta\omega$ of the peaks account for the difference $\Delta d_{hkl}$ between the layer and substrate lattice spacing. XRD do not directly provide the strain value on the crystal lattice. Te measurable quantities being the lattice mismatches $\Delta a_{\perp}/a_o$ and $\Delta a_{II}/a_o$, i. e $f_{\perp}$ and $f_{II.}$ The relationship between lattice mismatch components and misfit *f* with respect to substrate is:

$$f = f_{\perp}\,(1\text{-}\nu)/(1+\nu) + 2\,\nu\, f_{II}/\,(1+\nu) \tag{3.1.2}$$

where ν is the Poisson ratio
This is the basic equation for the strain and composition characterization of heterostructures for cubic lattice materials. In the case of semiconductor alloys $A_xB_{1-x}$ the composition *x* can be obtained if the relationship between composition and lattice constant is known. Poisson ratio is also composition depending and the use of Poisson ratio ν is only valid for isotropic materials. For a cubic lattice, it can only be applied for high symmetric directions as (001), (011), (111), but Poison ratio may be different along different directions ($\nu \approx 1/3$ for the most semiconductors alloys).
XRD can easily be employed to measure the lattice parameter with respect the substrate used as a reference. The strain and the composition of layer can be accurately determined if the dependence of the lattice parameter with the composition is known, the accuracy being mainly due to the precise knowledge of the lattice parameter –composition dependence.
In many cases a good approximation of a such dependence is given by Vegard law, which assumes that in the alloy $A_xB_{1-x}$ the lattice of the alloy is proportional to the stoichiometric coefficient *x*:

$$a\,(x) = x a(\mathrm{A}) + (1\text{-}\,x)\,a(\mathrm{B}) \tag{3.1.3}$$

From this equation the stoichiometric coefficient *x* is obtained:

$$x = (a(x) - a(B))/\ (a(A) - a(B)) \tag{3.1.4}$$

If $a$(B) is the substrate lattice parameter, the composition $x$ can be calculated from the measurement misfit f($x$) value:

$$x = f(x)/f(AB) \tag{3.1.5}$$

Where:
$f(x)$ is the measured misfit value with respect to $a$(B) and
$f$(AB) is the misfit between compound A and compound B, used as reference.
In the case of $GaAs_{1-x}N_x$ and $In_xGa_{1-x}As_{1-y}N_y$ dilute nitride alloys relationship between lattice parameters and composition assuming Vegard's law are the foolowing:

$$a_{GaAs1-xNx} = x\ a_{GaN} + (1- x)\ a_{GaAs} \tag{3.1.6}$$

$$a_{\ InxGa1-xAs1-yNy} = x\ y a_{InN} + (1- x)y\ a_{GaN} + x(1- y)\ a_{InAs} + (1- x)\ (1- y)\ a_{GaAs} \tag{3.1.7}$$

The lattice parameter measurements method is one of the most accurate way to determine the composition, provided that the composition versus lattice parameter dependence is known. The comparison between composition values obtained from XRD and that, determined by other analytical techniques has allowed to measure the deviation from the linear Vegard's law in alloys.
Table 1. presents the values of elastic constants and lattice parameters for GaAs, InAs, GaN, InN binary compounds.

| compound / Parameter | GaAs | InAs | GaN | InN |
|---|---|---|---|---|
| $C_{11}$, GPa | 118.79 | 83.29 | 293 | 187 |
| $C_{12}$, GPa | 53.76 | 45.26 | 159 | 125 |
| $a_{0,}$ nm | 0.5653 | 0.60584 | 0.4508 | 0.4979 |

Table 1. Elastic constants and lattice parameters for some III-V compounds

## 4. Low-temperature LPE growth

Low-temperature LPE is the most simple, low cost and safe method for high-quality III-V based heterostructure growth. It remains the important growth technique for a wide part of the new generations of optoelectronic devices, since the competing methods, MBE and MOCVD, are complicated and expensive although they offer a considerable degree of flexibility and growth controllability. The lowering the growth temperature for Al-Ga-As system provides the minimal growth rate values of 1–10 Å/s, and they are comparable with MBE and MOCVD growth values (Alferov et al, 1986). At the early stages of the process two-dimensional layer growth occurs, which ensures structure planarity and makes it possible to obtain multilayer quantum well (QW) structures (Andreev et al, 1996).

The results of study the crystallization process in the temperature range 650-400 °C demonstrate precise layer composition and thickness controllability for the low-temperature LPE growth. A necessary requirements for successful devices fabrication is the optimal doping of the structure layers at low temperatures. The experiments (Milanova and Khvostikov, 2000) on doping using different type dopants covered large range of carrier concentrations: from $10^{16}$ to $10^{19}$ $cm^{-3}$ for n $Al_xGa_{1-x}As$ layers ($0 \leq x < 0.3$); from $5 \times 10^{17}$ $cm^{-3}$ to well above $10^{19}$ $cm^{-3}$ for p $Al_xGa_{1-x}As$ ($0 \leq x < 0.3$); and from $10^{16}$ to $10^{18}$ $cm^{-3}$ for n- and p $Al_xGa_{1-x}As$ ($0.5 < x < 0.9$) layers. High quality multilayer heterostructures containing layers as thin as 2-20 nm, as well as several microns thick, with a smooth surface and flat interfaces have been grown by low-temperature LPE. The lowest absolute threshold current of 1.3mA (300 K) was obtained for buried laser diodes with a stripe width of ~ 1μm and cavity length of 125μm (Alferov et al, 1990).

High-efficiency solar cells for unconcentrated (Milanova et al, 1999) and concentrated solar cells (Andreev et al, 1999) have been fabricated by low-temperature LPE. The record conversion efficiency under ultra-high (>1000) concentration ratio solar radiation heve been achieved for GaAs single-junction solar cells based on multilayer AlGaAs/GaAs heterostructures (Algora et al, 2001).

The success of the LPE method is strongly depend on the graphite boat design used for epitaxy growth. The most widely used for LPE growth is a slide boat method. The conventional simple slide boat consists of a boat body in which are formed containers for liquid phase and a slider with one or more sits for the substrate (Fig. 4.1.). The slider moves the substrates under and out of the growth melt. This boat design has some disadvantages: the melt thicknesses is several millimeters and during growth from such semi-limited liquid-phase a portion of dissolved materials can not reach the substrate surface and forms stable seeds at a distance of 1 mm and more from the growth surface which deteriorate the planarity of the grown layer.

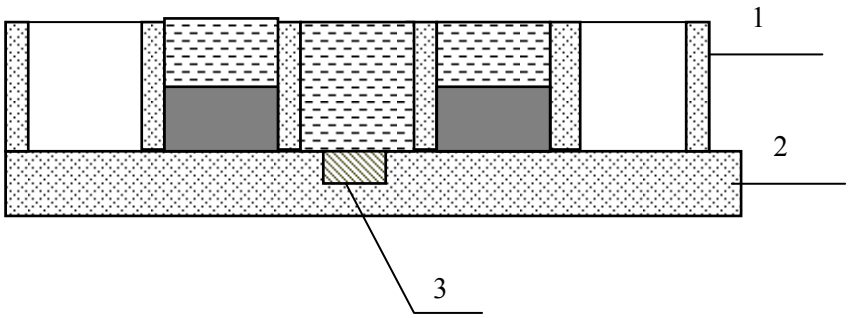


Fig. 4.1. Conventional slide boat for LPE growth: 1, body boat; 2, slider, 3, substrate.

Another drawback is the arising the defects on the layer surface due to the mechanical damage during its transfer from one melt to another. Also always on the surface of the melt present oxides films and it is difficult to completely removed these films even by long high-temperature baking. This is a critical problem for wetting of the substrate surface, especially for epitaxial process in Al-Ga-As system. A piston growth technique has been developed for LPE growth of AlGaAs heterostructures by Alferov at al (Alferov et al, 1975).

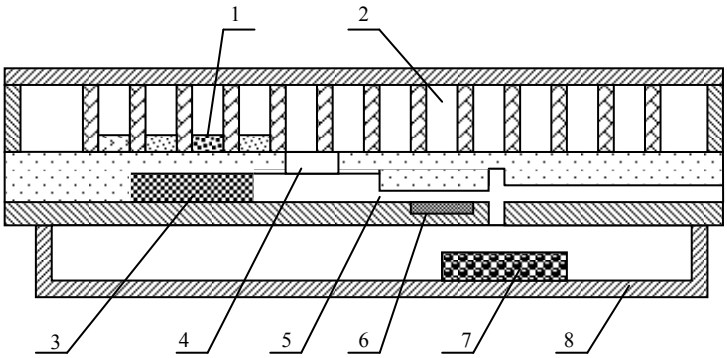


Fig. 4.2. Piston boat for growth of multilayer AlGaAs/GaAs heterostructures: 1, growth solution; 2, container for solution; 3, piston; 4, opening; 5, narrow slit; 6, substrate; 7, used solution; 8, container for used solutions.

The substrate surface in this boat after the first wetting is always covered by a melt and this solves difficulties of wetting during the growth of AlGaAs heterostructures in the range 600-400 °C. The piston boat design is shown in Figure 4.2. In this boat the melts of different compositions are placed in containers which can move along the boat body. The liquid phase falls down into the piston chamber and squeezes throw narrow slit into the substrate which allows mechanical cleaning of oxides films from liquid phase and insures a good wetting. The crystallization is carried out from the melt 0.5-1 mm thick. After the growth of the layer liquid phase is removed from the substrate by squeezing of the next melt. The last liquid phase is swept from the surface by shifting the substrate holder out side the growth chamber.

The liquid phase can not remove completely from the surface structure and cause a poor morphology of the last grown layer. The excess melt could be remove from the substrate by using additional wash melt, which may either has a poor adhesion to the substrate or may be relatively easy remove with post-growth cleaning and etching in selective etchants. Authors (Mishurnyi at al, 2002) suggest an original method to complete remove the liquid solution after epitaxy. The remained liquid phase is pulled up into the space between the substrate and vertical plates made of the same materials as the substrate assembled very closely to the substrate surface. This method is very useful for growth of multilayer heterostructures not containing Al in modified slide boat because prevent mixing of any liquids remaining. For the most multicomponent alloys such as InGaAsP, InGaAsSb, InPAsSb etc., lattice constant is very sensitive to composition variation and the piston boat is not suitable for their growth because of mixing of two deferent solutions. Slide boats with different design are used for fabrication of complicated multilayer heterostructure on the base of these multicomponent alloys. In order to improve the control of layer thicknesses and uniformity it is necessary the growth to be carried out using a finite melt. In this boat the liquid phase after saturations is transferred into the additional containers or growth chamber with finite space for the liquid phase. Figure 4.3 shows a schematic slide boat for epitaxy growth from finite melt.A critical requirement for the most multicomponent alloys, instead of AlGaAs, AlGaP, is precise determination of the growth temperature. The

temperature at the interface between the liquid phase and substrate can not be measured and common it is determined by measurements of the source component solubility (Mishurnyi et al, 1999) .

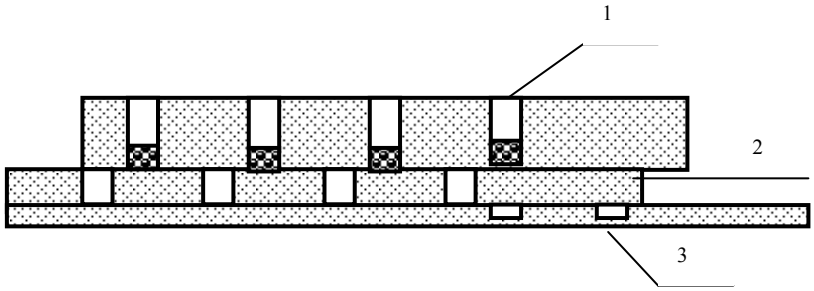


Fig. 4.3. Slide boat for growth from finite melt: 1, boat body with container for melts; 2, slider with container for finite melts; 3, slider for the substrates.

Slide boats with different design modification are used for growth of variety structures in different multicomponent system. A boat made of two different materials, sapphire (for body) and graphite (for slider), is suggested by Reynolds and Tamargo (Reynolds and Tamargo, 1984). This design reduces temperature variations around the perimeter of the substrate which contribute to unwanted 'edge' growth effects. Slide boats with narrowed melt contact for epitaxy of extremely thin epilayers have been used to grow active layer in single-quantum well lasers by (Alferov et al, 1985 ) and later by (Kuphal, 1991). Also a modified slide boat can be used for multilayer periodic structures growth (Arsent'ev et al, 1988). The use of two growth chambers with narrow slits makes it possible to produce such structures by means of repeated reciprocating movements of the slider with the substrate situated underneath these slits. Another variant of an LPE boat (Mishurnyi et la, 1997), which is a combination of the 'sliding' and 'piston' designs has been used successfully to grow InGaAsSb, AlGaAsSb and various multilayer structures on the basis of these materials.

## 5. Low-temperature LPE growth and characterization of dilute nitride GaAsN and InGaAsN thick layers

Dilute nitride III-V-N alloys with nitrogen content in the range of few percent, such as GaAsN and InGaAsN, are of considerable interest for application in multijunction solar cells.

The incorporation of nitrogen into group V sublattice causes profound effect on the band gap and properties of the dilute nitride material strongly differ from those of the conventional III-V alloys. While in conventional alloys a smaller lattice constant increases the band gap, the mixing of GaAs with few molar percent of GaN leads to giant reduction of its band gap due to the smaller covalent radius and large electronegativity of N atoms. The large changes in the electronic structure in dilute III–V nitrides could be explained by the band anticrossing model (BAC). The interaction between the localized levels introduced by a highly electronegative impurity, such as N in $GaN_xAs_{1-x}$, and the delocalized states of the host semiconductor causes a restructuring of the conduction band into E+ and E− subbands, which in this case effectively lowers the conduction band edge of the alloy.

Figure 5.1. shows the relationship between the lattice constant and band-gap energy in some III-V semiconductor alloys. In the case of InGaNAs adding In to GaAs increases the lattice constant, while adding N to GaAs decreases the lattice constant. In the same time the incorporation of In and N in GaAs leads to reduction of the band gap energy in the new alloy. Consequently, by adjusting the contents of In and N in quaternary InGaNAs alloys can be grown lattice-matched to GaAs layers because In and N have opposing strain effects on the lattice and make it possible to engineer a strain-free band gap layers suitable for different applications.

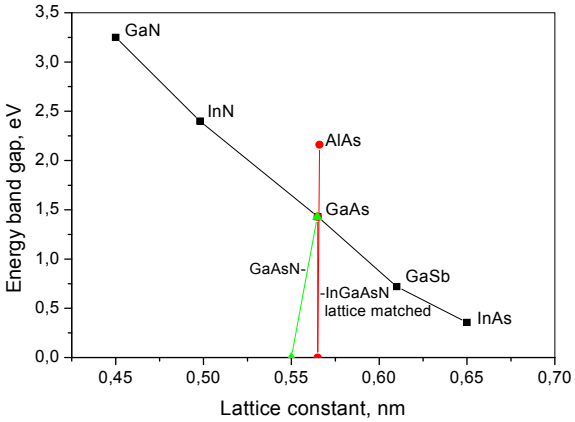


Fig. 5.1. Relationship between lattice constant and bad gap energy for some III-V semiconductor alloys

Recently a development of the spectral splitting concentrator photovoltaic system based on a Fresnel lens and diachronic filters has a great promise to reach super high conversion efficiencies (Khvostiokov et al. 2010). Module efficiency nearly 50% is expected for the system with three single-junction solar cells connected in series with band gap of 1.88-1.42-1.0 eV. The development of three optimized AlGaAs, GaAs and InGaAsN based cells is the best combination for application in such system if PV quality of the quaternary InGaAsN could be reached by LPE growth.

In this paper low-temperature LPE is proposed as a new growth method for dilute nitride materials. Because of its simplicity and low cost many experiments on GaInAsN and GaAsN growth under different condition and with different doping impurities could be made using LPE. The systematic study of their structural, optical and electrical properties by various methods make it possible to find optimized growth conditions for InGaAsN quaternary compounds lattice matched to GaAs substrate.

### 5.1 Growth and characterization of GaAsN layers

GaAsN compounds were grown by the horizontal graphite slide boat technique for LPE on (100) semi-insulating or n-type GaAs substrates. A flux of Pd-membrane purified hydrogen at atmospheric pressure was used for experiments. No special baking of the system was done before epitaxy. Starting materials for the solutions consisted of 99.9999 % pure Ga, polycrystalline GaAs and GaN. The charged boat was heated at 750°C for 1 h in a purified $H_2$ gas flow in order to dissolve the source materials and decrease the contaminants in the

melt. Epitaxial GaAsN layers 0.8-1.5 thick were grown from different initial temperatures varied in the range 560-650 $^{o}$C at a cooling rate of 0.6 $^{o}$C/min.

### 5.1.1 Structural characterization

XRD and SIMS techniques are used to determine N concentration in grown samples.
While SIMS measures the total nitrogen content in the layer, XRD determines the change in the lattice constant due to the substitution of nitrogen atoms on As-sublattice sites.
The N composition from XRD results could be estimated assuming Vegard's law. In many cases the Vegard's law is a good approximation for the lattice parameter dependence on the composition. The deviation from Vegard's law dependences on many parameters, for instance, the difference in the atom bond length, different atom electronegativity and elastic constants of the components in the alloy. For the ideal case N incorporates predominantly as substitutional $N_{As}$ atoms in As- sublattice substituting As atoms. However, it is known that there are some other N configurations: N-As split interstitial; N-N split interstitial; and isolated N interstitial. Figure 5.2 presents the main configurations of N in GaAsN as substitutional atom $N_{As}$ and as As-N and N-N split interstitials, respectively.
The influence of these N-related complexes on the lattice constant can be calculated on the base of the theoretical model of Chen (Chen et al. 1996) for analyzing the correlation between lattice parameters and point defects in semiconductors. According this model the lattice strain caused by the substitutional $N_{As}$ is given by the following relation:

$$\frac{\Delta a}{a} = \mu \frac{x(r_N - r_{As})}{2(r_{Ga} + r_{As})} \tag{5.1.1}$$

where: $r_{N,}$ $r_{Ga,,}$ $r_{As}$ the covalent radii;
$\mu = (1+\nu)/(1-\nu)$ , and v is the Poissn ratio
The lattice strained caused by split interstitial is:

$$\frac{\Delta a}{a} = \mu \frac{x(d_b - r_{Ga} - r_{As})}{2(r_{Ga} + r_{As})} \tag{5.1.2}$$

Where $d_b$ is the distance of the N-As complex from its nearest neighbours:

$$d_b = \frac{\sqrt[3]{3}}{3} r_{si} + \sqrt{(r_{si} + r_{Ga})^2 + \frac{2}{3} r_{si}^{\,2}} \tag{5.1.3}$$

where $r_{si}$ =( $r_N$ + $r_{As}$)/2 is an effective bond radius.

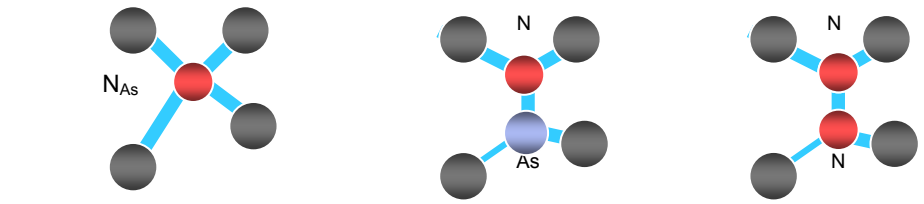


Fig. 5.2. The main configurations of nitrogen atoms in GaAsN
N-atom, As-atom Ga-atom

The effect of N-N interstitial is very small and can be neglected. Also the formation of an isolated N interstitial is unlikely due to a high formation energy (Li et al. 2001) and their concentrations in GaAsN is very small. While the substitutional $N_{As}$ atoms compress the lattice constant , the N-As complexes expand the lattice constant of GaAsN in the growth direction, as shown in Figure 5.3. So, XRD results may underestimated the N composition due to the N-As and N-N split interstitials.

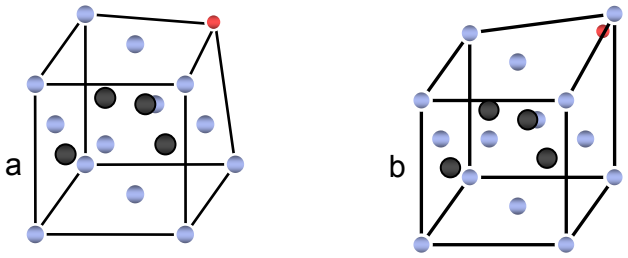


Fig. 5.3. Incorporation of N-atom in As-sublattice: a) as substitutional atom $N_{As}$; b) as As-N split interstitial

XRD rocking curves are recorded in the symmetrical (004) reflection. Fig. 5.4 shows the experimental XRD rocking curves of two GaAsN samples, 1.2 μm thick, with N composition of 0.3% and 0.62% and may consider that they are fuly relaxed. The N content determines the line shape of the main peak of the spectra: it manifests itself as a broad shoulder evolving into a weak separate peak shifted away to the right from the (004) GaAs substrate reflection. Our data show that N compositions measured by the two methods, SIMS and XRD, agree well and XRD measurements by using Vegard's law could be used to determine the lattice constant of GaAsN layers containing low N concentrations. These results are in a good agreement with the calculations from the theoretical model and the experimental results for small N concentration in the GaAsN reported in the literature. The deviation from Vegard's law has been observed for nitrogen concentration levels above 2.9 mol % GaN in the layer ( Spruytte at all., 2001; Li et al. 2001).

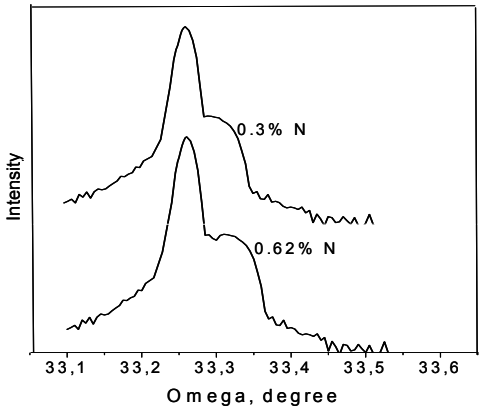


Fig. 5.4. XRD rocking curves for GaAsN samples with differenrt N content.

Unlike XRD used for assessing the incorporation of nitrogen in $GaAs_{1-x}N_x$ alloys grown by LPE the nitrogen bonding configurations and local atomic structures have been studied using x-ray photoelectron spectroscopy (XPS) and Fourier transform infrared (FTIR) spectroscopy. The XPS spectra have been measured over a range of binding energies from 1 to 550 eV. The X-ray photoelectron spectra of N 1s photoelectron and Ga LMM Auger lines recorded from the as grown $GaAs_{1-x}N_x$ samples prepared in different temperature ranges are shown in Fig 5.5. It is clearly seen the Ga Auger peak around 391 eV and the N 1*s* level photoemission peak of the samples. The variation of the intensity of the N 1*s* peak with respect to the Ga LMM peaks reflects is due to the different nitrogen content of the samples. Sample grown from higher initial epitaxy temperature of 650 $^{o}$C contains 0.2% N and exhibits a N 1s peak with lower intensity and lower binding energy in comparison with the N 1s peak intensity of the sample grown in the lower temperature range (600-570 $^{o}$C) with 0.5% N content. It has been established that lower epitaxy temperatures favours nitrogen incorporation in the layers. The N 1s spectra of the samples indicate that nitrogen atoms exist in a single-bonded configuration, the Ga-N bond, and interstitial nitrogen complexes is not observed, in contrast to data of high nitrogen content GaAsN samples where the additional nitrogen complex associated peak is recorded (Spruytte at all., 2001).

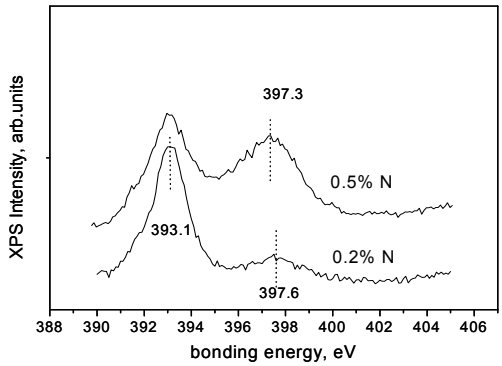


Fig. 5.5. XPS spectra of two GaAsN samples with different N content.

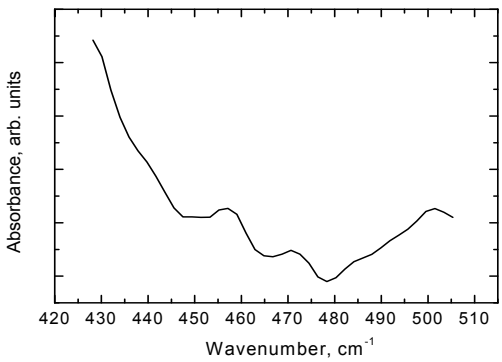


Fig. 5.6. FTIR spectrum of as grown GaAsN sample.

FTIR absorption spectra of an as grown $GaAs_{1-x}N_x$ layer on a n-GaAs substrate is plotted in Fig. 5.6. A peak at 472.6 $cm^{-1}$, attributed to a local vibrational mode of nitrogen at arsenic site in GaAs is clearly seen.

### 5.1.2 Electrical characterization

Electrical parameters of undoped GaAs and GaAsN layers with different nitrogen content grown on seminsulating (001) GaAs substrates are measured in the temperature range 80 – 300 K using van der Pauw geometry.

Figure 5.7. shows the temperature dependence of the Hall-concentration $n_H$ on reciprocal temperature for two layers GaAsN with nitrogen concentration of 0.2% and 0.5%, respectively in comparison with undoped GaAs. It is seen that all samples are of n-type and for layers containing nitrogen electron concentration increases about one order of magnitude. This could be explained by the assumption that nitrogen behaves mainly as an isoelectronic donor, which arises from the local heterojunction scheme GaAs-GaN according to Belliache (Bellaiche et al., 1997). The results shown in figure indicate that the free carrier concentration increases strongly with the N concentration. The increase in $n_H$ has also been observed in $GaN_xAs_{1-x}$ doped with S (Yu et al., 2000a) and in $Ga_{1-3x}$ $In_{3x}NxAs_{1-x}$ alloys doped with Se (Skierbiszewski at al., 2000). This large increase of the free electron concentration can be quantitatively explained by a combination of the band anticrossing model (Shan et al, 1999) and the amphoteric defect model (Walukiewicz, 1989). The later suggests that the maximum free carrier concentration in a semiconductor is determined by the Fermi energy with respect to the Fermi-level stabilization energy $E_{FS}$ which is a constant for III-V semiconductors. Since the position of the valence band in GaAsN is independent of N concentration, the giant downward shift of the conduction band edge toward $E_{FS}$ and the enhancement of the density of states effective mass in GaAsN lead to much larger concentration of uncompensated, electrically active donors for the same location of the Fermi energy relative to $E_{FS}$. In order to explain the large enhancement of the doping limits in dilute nitride alloys both the effects of band gap reduction and the increase in the effective mass have to be taken into account (Yu et al., 2000 b; Skierbiszewski at al., 2000).

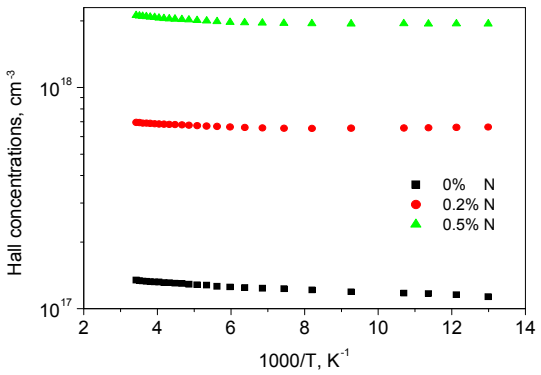


Fig. 5.7. Free carrier concentration as a function of inverse temperature for as grown GaAs, and two GaAsN layers with different N content

Figure 5.8. presents the temperature dependencies of the Hall-mobility for the same samples. The mobility of the dilute GaAsN samples is considerably lower due to space charge scattering contributions induced by N-related defects added to well-known scattering mechanisms such as phonon and ionized impurity scattering. The mobility maximums of both curves are almost at the same temperature with a relatively small difference of about 20K, which is an indication for scattering specificity. It is seen a well expressed low-temperature mobility decrease which could be explained by the temperature dependence of the GaAs conduction band edge energy, which is closer to the N defect levels at lower temperatures, increasing the scattering cross-section.

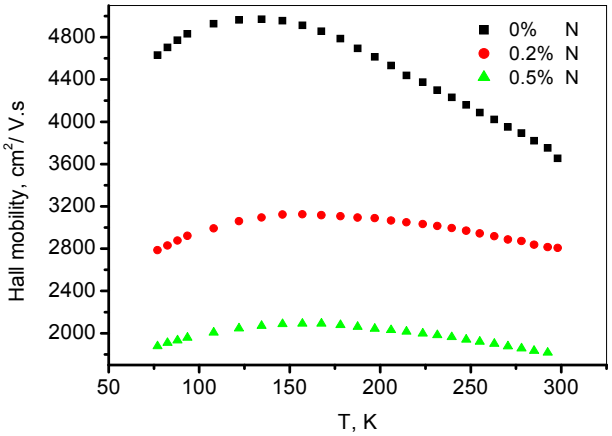


Fig. 5.8. Temperature dependence of Hall electron mobility for GaAs (full squares), and two GaAsN with: 0.2%N (full circles); 0.5%N (full triangles)

The mobility values of the dilute GaAsN samples is lower than those of the undoped GaAs layer but considerable higher than mobility values obtained in n-type GaAsN films with similar free electron concentration grown by MOCVD and MBE.

### 5.2 Growth and characterization of InGaAsN layers

Dilute InGaAsN layers have been prepared using the same technique as for GaAsN growth. A series of nearly-lattice matched InGaAsN epilayers 1.3-1.5 μm thick have been grown from In-rich solution containing 1.5 at.% polycrystalline GaN as a nitrogen source in the temperature range 615 – 580 °C at a cooling rate 0.6 °C/min.

#### 5.2.1 Structural characterization

Typical XRD rocking curves for grown layers are plotted in the Fig. 5.9.
Two prominent peaks associated with the GaAs substrate and the quaternary InGaAsN layer are observed. The lattice mismatch $\Delta a/a_o$ determined from the XRD spectrum is ~ 0.1%. The *In*-concentration of the layers measured separately by X-ray microanalyses is 6.4%. Using Vegard's law the *N*- content in InGaAsN layers is determined to be 2.8%

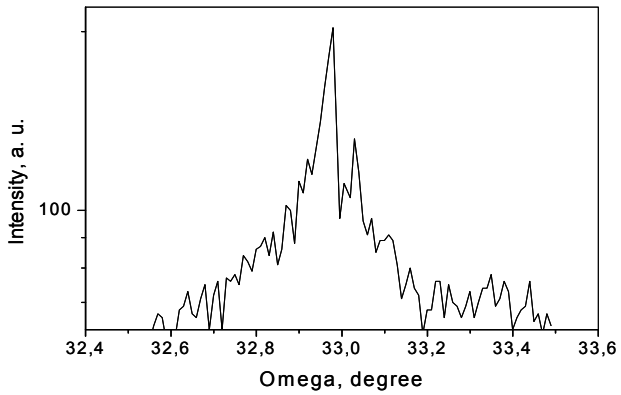


Fig. 5.9. XRD rocking curves of InGaAsN sample

The local structure of the InGaAsN is defined by Raman spectrum. In the Raman spectrum, presented in fig. 5.10. does not observed N-induced local mode LO2 , assigned to the vibration of isolated nitrogen atom bonded to four Ga neighbors ($N_{As}Ga_4$). Instead of this two LVM peaks at 454 and 490 $cm^{-1}$ originated from In-N bonds in a local $Ga_3In_1$-N or $Ga_2In_2$-N configurations are appeared. Similar LVM peaks have been reported in the literature for as grown InGaAsN layers by MBE (Mintairov et al., 2001, Hashimoto et al., 2003) and for some MBE and MOCVD samples after annealing (Pavelescu et al.,2005; Kurtz et al. 2001). The experimentally observed local modes could be explained by theoretical analyses of the microscopic lattice structures related to the incorporation of N in InGaAsN alloys. The Monte Carlo simulation (Kim & Zunger, 2001) reveal that in InGaAsN quaternary alloys the "small atom–large atom" bond configuration i.e. "large cation-small anion" In-N + "small cation-large anion" Ga-As is preffered for better lattice-matched of the alloy to GaAs substrate, because introduces less strain. On the other hand, the cohesive energies of GaN is larger than that of InN, so the highly strained Ga-N + In-As configuration is preferred in terms of bond energy. In LPE growth under near to equilibrium conditions In-N bonds are more favorable since they reduce the sum of local strain plus chemical bond energies. The introduction of In changes N environment by formation short-range-ordered nitrogen centered N-$In_nGa_{4-n}$ ($0 \le n \le 4$) clusters in InGaAsN alloy. In Ga-rich InGaAsN quaternary the most probably realized are the nearest –neighbor pair defects $N_{As}$-$In_{Ga}$ in which one of the Ga atom in the neighborhood of N is replaced by a large size heavier $In_{Ga}$ ($N_{As}In_{Ga}Ga_3$) and also a formation of a second nearest-neighbor complex $N_{As}In_{Ga}(2)Ga_2$ where two of four Ga atoms is replaced by two large-site and heavier $In_{Ga}$ in the vicinity of $N_{As}$. The calculations using Green's function technique (Talwar, 2007) relieve the splitting of a triple degenerate $N_{As}$ near to 471 $cm^{-1}$ into a non-degenerate LVM ~ 462 $cm^{-1}$ and a double degenerate LVM at 490$cm^{-1}$ for the nearest –neighbor complex and three bands near to 481, 457, and 429 for second nearest-neighbor complex . The surface roughness of the samples has been examined by atomic force microscopy (AFM). A three-dimensional AFM image of an as grown 1.3 μm-thick InGaAsN layer is presented in Fig. 5.11. The measured root-mean-square (RMS) roughness on 1-micron area is 0.42 nm.

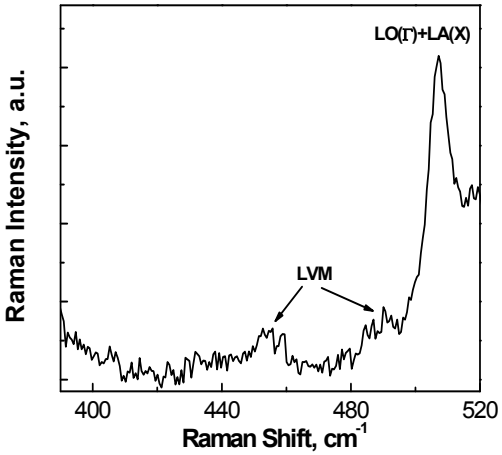


Fig. 5.10. Raman spectrum of as grown InGaAsN layer.

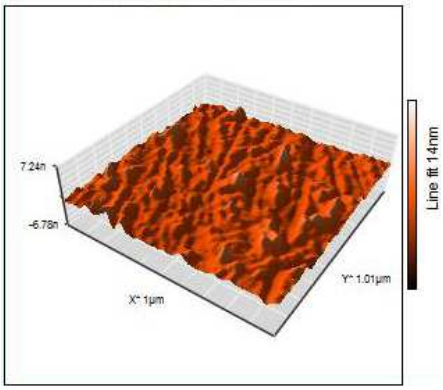


Fig. 5.11. AFM image of the surface of as grown InGaAsN.

### 5.2.2 Electrical characterization

In the Fig. 5.12 are plotted the temperature dependence of Hall concentrations $n_H$ for lattice matched InGaAsN in comparison with a metamorphic InGaAs layer. For undoped InGaAs, $n_H$ decreases linearity in the explored temperature range, 80 to 300K, typical for slightly degenerate III-V semiconductors. However, for N-containing films, two distinct temperature regimes with different temperature dependence of $n_H$ are observed. The Hall electron concentration decreases as the temperature decreases down to about 200 K, indicating the presence of thermally activated deep donor levels within the dilute nitride bandgap. The saturation of $n_H$ at low temperature (T < 200K) is attributed to fully ionized shallow donors. This behavior could be explained by the presence of two donor levels in the InGaAsN bandgap, one being a shallow N isoelectronic donor and the second a thermally activated deeper donor, presumably N-related deep-level defects typically associated with different N-N pair and N-cluster states ( Zhang & Wei, 2001).

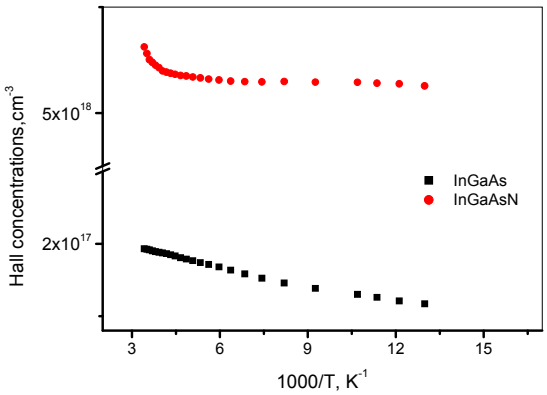


Fig. 5.12. Temperature dependence of free carrier concentrations for undoped InGaAs and lattice matched InGaAsN samples

The temperature dependence of Hall mobility for undoped InGaAs and InGaAsN layers grown from In-rich solution is similar to those for the GaAsN layers grown from Ga-rich solution as it is shown in Figures 5. 13 and 5. 14.

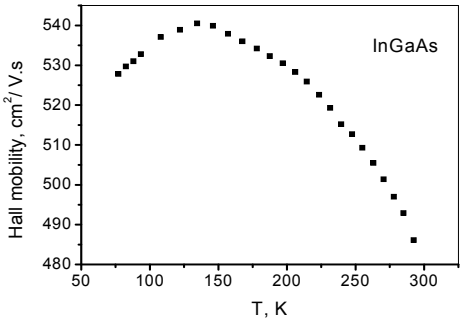


Fig. 5.13. Hall mobility as a function of temperature for undoped InGaAs sample

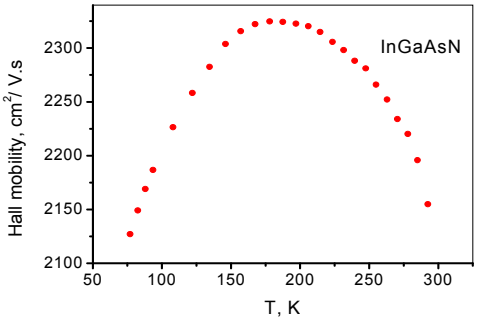


Fig. 5.14. Hall mobility as a function of temperature for lattice matched InGaAsN sample

The mobility of the metamorphic InGaAs structure is low, down to 500 $cm^2/V.s$, since it possibly contains threading dislocations of high density and the latter causes relatively poor material quality. High values over 2000 $cm^2/$ V.s for Hall mobility exhibits the lattice matched to GaAs substrate InGaAsN sample. These values are about the theoretical limit predicted by Fahy and O'Reilly (Fahy and O'Reilly, 2004) and among the highest reported for lattice matched thick InGaAsN layers.

## 6. Conclusion

Dilute nitride GaAsN and InGaAsN epitaxial layers have been prepared by low-temperature LPE using polycrystalline GaN as a source for nitrogen. The GaAsN layers, 0.8-1.5 μm thick, with 0.15-0.6 at. % N content in the solid have been grown from different initial epitaxy temperature varied in the range 650-550 °C. The lowering the epitaxy temperatures favors nitrogen incorporation in the layers. The Hall measurements reveal sharply increase of free carrier concentrations about one order of magnitude and decrease of Hall mobility for GaAsN samples in comparison with undoped GaAs.

Lattice-matched conditions for coherent growth of InGaAsN layers on GaAs have been found. The results suggest preferential In-N bond formation for high quality growth of these alloys. Temperature dependent electronic transport measurements show a thermally activated increase in the free carrier concentration at measurement temperatures higher than 200 K, suggesting the presence of carrier trapping levels below the GaAsN conduction band edge. Nearly lattice matched to GaAs substrate thick $In_xGa_{1-x}As_{1-y}N_y$ (x~ 6.4%, y~2.8%) layers exhibit high values over 2000 $cm^2/$ V.s for Hall electron mobility.

Further study is necessary in order to determine the potential of melt-grown quaternary InGaAsN alloys for solar cell application. This will be attained by: study the influence of growth conditions on the material quality in wide temperature range 450-600 °C and differentiation between intrinsic and extrinsic limitations for device performance; finding optimized growth conditions for InGaAsN lattice matched to GaAs with improved material quality ; extending the long-wavelength limit of GaAsN-based materials by the lowering the band gap energy of dilute nitride structure that can be lattice matched grown on GaAs.

The finale goal is a development of single-junction solar cells with high photovoltaic parameters.

## 7. References

Alferov Zh.I., Andreev V.M., Konnikov S.G., Larionov V.R. and Shelovanova G.N. (1975). Investigation of a new LPE method of obtaining Al-Ga-As heterostructures, *Kristall Technik*, Vol.10, No 2, pp 103-110.

Alferov Zh.I., Garbuzov D.Z., Arsent'ev I.N., Ber B.Ya., Vavilova L.S., Krasovskii V.V. and Chydinov A.V.(1985) Auger profiles of the composition and luminescence studies of liquid-phase grown InGaAsP

Alferov Zh.I., Andreev V.M., Vodnev A.A., Konnikov S.G., Larionov V.R., Pogrebitskii K.Yu. Rymiantsev V.D. and Khvostikov V.P.(1986). AlGaAs heterostructures with quantum-well layers, fabricated by low-temperature liquid-phase epitaxy, *Sov. Tech. Phys. Lett.*, 12(9), 450–451.

Alferov Zh.I., Andreev V.M., A.Z. Mereutse, Syrbu A.V., Suruchanu G.I. and Yakovlev V.P.(1990). Super low-threshold (Ith = 1.3 mA, T= 300 K) quantum-well AlGaAs

lasers with uncoated mirrors prepared by liquid-phase epitaxy, *Sov. Tech. Phys. Lett.*, Vol.16, No 5, pp 339–340.

Algora C., Oritz E., Rey-Stolle I, Diaz V., Pena R., Andreev V. M., Khvostikov V. P., Rumyantsev V. D.(2001). A GaAs solar cell with an efficiency of 26.2% at 1000 suns and 25.0% at 2000 suns, *IEEE Trans. on Elec. Dev.*, Vol. 48, No 5, pp 840-844. ISSN: 0018-9383.

Andreev V. M., Kazantsev A. B., Khvostikov V. P., Paleeva E. V., Rumyantsev V. D. and Sorokina S. V. (1996). Quantum-well AlGaAs heterostructures grown by low-temperature liquid-phase epitaxy, *Materials Chemistry and Physics*, Vol. 45, No 2, p p.130-135.

Andreev V. M., Khvostikov V. P., Larionov V. R., Rumyantsev V. D., Paleeva E. V., Shvarts M. Z.(1999). High-efficiency AlGaAs/GaAs concentrator (2500 suns) solar cells *Fiz. Tekh. Poluprovodn*. Vol. 33, N0 9, pp 1070-1072.

Arsent'ev I.N., Bert N.A., Vasil'ev A.V., Garbuzov D.Z., Zhuravkevich E.V., Konnikov S.G., Kosogov A.O., Kochergin A.V., Faleev N.N. and Flaks L.I.(1988). Periodic multilayer In-Ga-As-P structures fabricated by liquid-phase epitaxy, *Sov. Tech. Phys. Lett.*, Vol 14, No 4, pp 264–266.

Ayers J.E., Schowalter L.J., and S.K. Ghandhi (1992). Post-growth thermal annealing of GaAs on Si(001) grown by organometallic vapor phase epitaxy, *J. Cryst. Growth*, Vol. 125, No1-2, pp. 329-335.

Bauer, E . (1958). Phaenomenologische Theorie der Kristallabscheidung an Oberflaechen, *Zeitschrift für Kristallographie*, Vol. 110, pp 372-394.

Bellaiche L., S. H. Wei, Zunger A., (1997) Band gaps of GaPN and GaAsN alloys, *Appl. Phys. Lett.*, Vol. 70, No 26, pp.3558-3560.

Chen N. F., Wang Y., He H, and Lin L. (1996). Effects of point defects on lattice parameters of semiconductors, *Physical Review B*, Vol. 54, No 12, (September 1996), pp 8516-8521.

Dhar S., Halder N., Mondal A., Bansal B., Arora B. M. (2005). Detailed studies on the origin of nitrogen-related electron traps in dilute GaAsN layers grown by liquid phase epitaxy, *Semiconductor Science and Technology*, Vol. 20, No. 12. pp. 1168-1172.

Fahy S., O'Reilly E. P. (2004), Theory of electron mobility in dilute nitride semiconductors, *Physica E*: *Low-dimensional systems and nanostructures*, Vol. 21, No 1-2, pp. 881-885.

Frank F.C. and Van der Merwe J.H. (1949). One-dimensional dislocations. II. Misfitting monolayers and oriented overgrowth, *Proc. R. Soc. London A*, Vol. 198, No 1053, ( August 15, 1949), pp 216 -225.

Grabow M.H. and Gilmer,G.H. (1988). Thin film growth modes, wetting and cluster nucleation, *Surf. Science*, Vol. 194, No 3, pp 333-346

Guter W., Schöne J., Philipps S., Steiner M., Siefer G., Wekkeli A., Welser E, Oliva E, Bett A. and Dimroth F.(2009). Current-matched triple-junction solar cell reaching 41.1% conversion efficiency under concentrated sunlight, *Appl. Phys. Lett*. Vol. 94, No 2, 023504.

Johnston S. W., Kurtz S. R., Friedman D. J., Ptak A. J., Ahrenkiel R. K., and Crandall R. S. (2005). Observed trapping of minority-carrier electrons in *p*-type GaAsN during deep-level transient spectroscopy measurement, Appl. Phys. Lett. Vol 86, No 7, 072109.

Hashimoto A., Kitano T., Nguyen A.K., Masuda A., Yamamoto A., Tanaka S., Takahashi M., Moto A., Tanabe T., Takagishi S., Raman characterization of lattice-matched

GaInAsN layers grown on GaAs (001) substrates, *Solar Energy Materials & Solar Cells* 2003, Vol. 75, pp. 313–317.

Hiramatsu K., Itoh S., Amano H., Akasaki I., Kuwano N., Shiraishi T. and Oki K.(1991). Growth mechanism of GaN grown on sapphire with A1N buffer layer by MOVPE, *J. Cryst. Growth*, Vol.115, No 1-4 , (Desember,1991), pp 628-633.

Khan A, Kurtz S. R., Prasad S., Johnston S. W., and Gou J. (2007). Correlation of nitrogen related traps in InGaAsN with solar cell properties, *Appl. Phys. Lett.* Vol. 90, No 24, 243509.

Khvostikov V.P., Sorokina S.V., Potapovich N.S., Vasil'ev V.I., Vlasov A.S., Shvarts M.Z., Timoshina N.Kh., Andreev V.M., (2010). Single-junction solar cells for spectrum splitting PV system, *Proceedings of the 25th European PV Solar Energy Conference and Exhibition,* Valencia, Spain6-10 September 2010.

Kim K. and Zunger A., Spatial Correlations in GaInAsN Alloys and their effects on Band-Gap Enhancement and Electron Localization, *Phys. Rev. Lett.*, Vol. 86, No 12, pp. 2609-2612.

King R.(2008). Multijunction cells: record breakers, *NaturePhotonics*, Vol. 2, pp. 284– 285.

Krispin P., Spruytte S. G., Harris J. S., and Ploog K. H. (2002) Electron traps in Ga(As,N) layers grown by molecular-beam epitaxy, *Appl. Phys. Lett.* Vol. 80, No 12, pp 2120-2122.

Kuphal E. (1991). Liquid Phase Epitaxy, *Appl. Phys. A* 52, pp 380–409.

Kurtz S. R, Allerman A. A., Jones E. D., Gee J. M., Banas J. J., and Hammons B. E. (1999) InGaAsN solar cells with 1.0 ev band gap, lattice matched to GaAs, *Applied Physics Letters*, Vol. 74, No 5, pp. 729–731.

Kurtz S. R., Allerman A. A., Seager C. H., Sieg R. M., and Jones E. D. (2000), Minority carrier diffusion, defects, and localization in InGaAsN, with 2% nitrogen, *Applied Physis Letters*, Vol. 77, No 3, pp. 400–402.

Kurtz S., Webb J., Gedvilas L., Friedman D., Geisz J., Olson J., King R., Joslin D., & Karam N., *Appl. Phys. Lett.*, 2001, Vol. 78, No 6, pp. 748 -750.

Kurtz S. R., Klem J. F., Allerman A. A., Sieg R. M., Seager C. H., & Jones E. D. (2002) Minority carrier diffusion and defects in InGaAsN grown by molecular beam epitaxy, *Appl. Phys. Lett.*, Vol. 80, No 8, pp. 1379-1381.

Li W., Pessa M., & Likonen J. (2001) Lattice parameter in GaNAs epilayers on GaAs: Deviation from Vegard's law, *Appl. Phys. Lett.*, Vol. 78, No 19, pp. 2864-2866.

Mattes B.L. and Route R.K.(1974). LPE growth of GaAs: Formation of nuclei and surface terraces , *J. Cryst. Growth*, Vol. 27, (December 1974), pp 133-141.

Matthews J. W.& Blakeslee A. E. (1974). Defects in epitaxial multilayers: I. Misfit dislocations, *J. Cryst. Growth*, Vol. 27, (December 1974) pp. 118-125.

Milanova M., Mintairov A., Rumyantsev V., Smekalin K.(1999). Spectral characteristics of GaAs solar cells grown by LPE, *J. of Electronic Mat.*, Vol 28, No 1, pp 35-37.

Milanova M. and Khvostikov V.(2000). Growth and doping of GaAs and AlGaAs layers by lowtemperature liquid-phase epitaxy, *J. Crystal Growth,* Vol. 219, No 10, pp 193–198.

Milanova M., Kakanakov R., Koleva G., Arnaudov B., Evtimova S., Vitanov P., Goranova E.,. Bakardjieva Vl, Alexieva Z.(2009) Incorporation of nitrogen in melt grown GaAs , *J. Optoelectronics and Advanced Materials*, Vol. 11, No. 10, pp. 1471-1474.

Mintairov A. M., Blagnov P. A.,. Merzj J. L, Ustinov V. M. & Vlasov A. S. (2001). Vibrational study of nitrogen incorporation in InGaAsN alloys, *9th Int. Symp. "Nanostructures: Physics and Technology"* NC.13p, St Petersburg, Russia, June 18-22, 2001.

Mishurnyi V.A., de AndaF., Gorbatchev A.Yu., Vasil'ev V.I., Faleev N.N.(1997). InGaAsSb growth from Sb-rich solutions, *J. Crystal Growth,* Vol. 180, pp 34–39.

Mishurnyi V.A., de Anda F., Hernandes del Castillo I.C. and Gorbatchev A.Yu.(1999). Temperature determination by solubility measurements and a study of evaporation of volatile components in LPE, *Thin Solid Films,*Vol. 340, pp 24–27.

Mishurnyi V.A., de Anda F. and Gorbatchev A.Yu.(2002). Some problems on the phase diagrams research in LPE, *Current Top. Crystal Growth Res.*, Vol. 6, pp 115–125.

Nabetani Y., Ishikawa T., Noda S. and Sasaki A.(1994). Initial growth stage and optical properties of a three-dimensional InAs structure on GaAs, *Journal of Applied Physics*, (July, 1994) Vol. 76, No 1, pp 347-351.

Nishimura K., Lee H.-S. , Suzuki H., Ohshita Y., & Yamaguchi M. (2007) Chemical Beam Epitaxy of GaAsN Thin Films with Monomethylhydrazine as N Source, *Jpn. J. Appl. Phys.,* Vol. 46, pp. 2844-2847.

Ohshita Y, N. Kojima T. Tanaka T. HondaM. Inagaki and M. Yamaguchi Novel material for super high efficiency multi-junction solar cells *J. Cryst. Growth*, Vol 38, No 1, (March 2011) pp 328-331.

Pavelescu E.-M., Wagner J., Komsa H.-P., Rantala T. T., Dumitrescu M.& Pessa M., Nitrogen incorporation into GaInNAs lattice-matched to GaAs: The effects of growth temperature and thermal annealing, *J. Appl. Phys.*, 2005, Vol.78, No 8, pp. 083524-1-4.

People R.& Bean J. C. (1985) Calculation of critical layer thickness versus lattice mismatch for $Ge_xSi_{1-x}$/Si strained-layer heterostructures, *Appl. Phys. Lett.*, Vol. 47, No 3, pp. 322-324.

Ptak A. J., Friedman D. J., Kurtz S., & Keihl J.(2005). Enhanced depletion width GaInNs solar cells grown by molecular beam epitaxy, *Proceedings of 31IEEE PVSC*, pp. 603–606, Orlando, Florida, USA, January 3-7, 2005.

Reynolds C.L. and Tamargo M.C. (1984) LPE appartus with improved thermal geometry, US Patent 4 470 368.

Scheel H.J.(2003) Control of Epitaxial Growth Modes for High-performance Devices, In: *Crystal Growth Technology*, Scheel H.J.& Fukuda T., pp. 623-642, John Wiley & Sons, Ltd.

Shan W, Walukiewicz W, Ager JW, Haller EE, Geisz JF, Friedman DJ, Olson JM, Kurtz SR. (1999) Band Anticrossing in GaInNAs Alloys. *Phys. Rev. Lett.*, Vol. 82, No 6, pp 1221–1224.

Sheldon P., Jones K.M., Al-Jassim M.M., & Yacobi B.G.(1988) Dislocation density reduction through annihilation in lattice-mismatched semiconductors grown by molecular beam epitaxy, *J. Appl. Phys.*, Vol. 63, No 11, pp. 5609-5611.

Skierbiszewski C., Perlin P., Wisniewski P., Knap W., Suski T., Walukiewicz W., Shan W., Yu K. M., Ager J. W., Haller E. E., Geisz J. F., and Olson J. M. (2000) Large, nitrogen-induced increase of the electron effective mass in $In_yGa_{1-y}N_xAs_{1-x,}$ *Appl. Phys. Lett.* Vol 76, No 17, pp 2409-2411.

Spruytte S. G., Coldren C. W., Harris J. S., Wampler W., Krispin P., Ploog K., & Larson M. C. (2001) Incorporation of nitrogen in nitride-arsenides: Origin of improved luminescence efficiency after anneal, *J. Appl. Phys.*, Vol. 89, No 8 , pp. 4401-4406.

Stranski I. N. and Krastanov L. V. (1939). *Abhandlungen der Mathematisch-Naturwissenschaft lichen Klasse.,* Akademie der Wissenschaften und der Literatur in Mainz, Vol. 146, p. 797.

Talwar D. N. (2007) Chemical bonding of nitrogen in dilute InAsN and high In-content GaInAsN, Phys. Stat. Sol. (c) Vol. 4, No. 2, pp. 674– 677.

Van der Merwe J.H (1979), Critical Reviews in Solid State and Materials Science, in *Chemistry and Physics of Solid Surfaces*, editor R. Vanselow, CRC Press, Boca Raton, 1979, 209 p.

Vitanov P., Milanova M., Arnaudov B., Evtimova S., Goranova E., Koleva G., Bakardjieva Vl. & Popov G. (2010) Study of melt-grown GaAsN and InGaAsN epitaxial layers (2010). *Journal ofPhysics:ConferenceSeries*, Vol. 253, pp. 012045-1-6.

Volmer M. & Weber A.,(1926). Keimbildung in übersättigten Gebilden, *Z. Physik Chem.*, Vol.119, pp 277-301.

Walukiewicz W., (1996) Amphoteric native defects in semiconductors, *Appl. Phys. Lett.*, Vol. 54, No 21, pp. 2094-2096.

Weyeres M., Sato M., & Ando H.(1992) Red shift of photoluminescence and absorption in dilute gaasn alloy layers, *Japanese Journal of Applied Physics*, Vol. 31, pp. L853.

Yamaguchi M., Nishimura K., Sasaki T., Suzuki H., Arafune K., Kojima N., Ohsita Y., Okada Y., Yamamoto A., Takamoto T. & Araki K. (2008). Novel materials for high-efficiency III-V multi-junction solar cells, *Solar Energy*, Vol. 82, No 2, pp. 173-180.

Yu K. M., Walukiewicz W., Shan W., J. Wu, Ager J. W., HallerE. E., Geisz J. F., & Ridgway M. C. (2000a). Nitrogen-induced enhancement of the free electron concentration in sulfur implanted $GaN_xAs_{1-x}$ , *Appl. Phys. Lett.* Vol. 77, No 18, pp 2858-2860.

Yu K. M., Walukiewicz, W., Shan W., Ager J. W., Wu J., Haller E. E., Geisz J. F., Friedman D. J. and Olson J. M. (2000b) Nitrogen-induced increase of the maximum electron concentration in group III-N-V alloys. *Phys. Rev. B*, Vol. 61, No 20, pp.R13337-R13340.

Zhang S. B.& Wei S. H. (2001). Nitrogen Solubility and Induced Defect Complexes in Epitaxial GaAs:N, *Phys. Rev. Lett.*, Vol. 86, No 9, pp. 1789–1792.

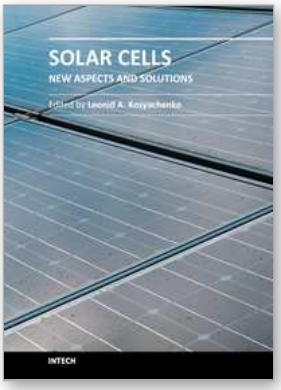


**Solar Cells - New Aspects and Solutions**

Edited by Prof. Leonid A. Kosyachenko

ISBN 978-953-307-761-1
Hard cover, 512 pages
**Publisher** InTech
**Published online** 02, November, 2011
**Published in print edition** November, 2011

The fourth book of the four-volume edition of 'Solar cells' consists chapters that are general in nature and not related specifically to the so-called photovoltaic generations, novel scientific ideas and technical solutions, which has not properly approved. General issues of the efficiency of solar cell and through hydrogen production in photoelectrochemical solar cell are discussed. Considerable attention is paid to the quantum-size effects in solar cells both in general and on specific examples of super-lattices, quantum dots, etc. New materials, such as cuprous oxide as an active material for solar cells, AlSb for use as an absorber layer in p-i-n junction solar cells, InGaAsN as a promising material for multi-junction tandem solar cells, InP in solar cells with MIS structures are discussed. Several chapters are devoted to the analysis of both status and perspective of organic photovoltaics such as polymer/fullerene solar cells, poly(p-phenylene-vinylene) derivatives, photovoltaic textiles, photovoltaic fibers, etc.



INTECH
open science | open minds

**InTech Europe**
University Campus STeP Ri
Slavka Krautzeka 83/A
51000 Rijeka, Croatia
Phone: +385 (51) 770 447
Fax: +385 (51) 686 166
www.intechopen.com

**InTech China**
Unit 405, Office Block, Hotel Equatorial Shanghai
No.65, Yan An Road (West), Shanghai, 200040, China
中国上海市延安西路65号上海国际贵都大饭店办公楼405单元
Phone: +86-21-62489820
Fax: +86-21-62489821